DEPÓSITO LEGAL ppi 201502ZU4666
*Esta publicación científica en formato digital*
*es continuidad de la revista impresa*
ISSN 0041-8811
DEPÓSITO LEGAL pp 76-654

# Revista de la Universidad del Zulia

Fundada en 1947
por el Dr. Jesús Enrique Lossada

## Ciencias Exactas Naturales y de la Salud

Año 11 N° 30
Mayo - Agosto 2020
Tercera Época
Maracaibo-Venezuela

# Drug delivery via super-paramagnetic $(N2)n[SiO2(OH)2]8$ Core-Shell catalyst

Somayeh Khosravi*
Majid Monajjemi**

ABSTRACT

The MNPs @ $[SiO_2(OH)_2]_8$ catalyzers were stablished via ab-initio and quantum mechanics & Molecular mechanic (QM/MM) simulation. The studies focus on how to improve the dispersion of composite particle for achieving high magnetic performances. The results revealed that the Fe3O4 @$[SiO_2\ (OH)_2]_8(N_2)_8$ as a cabalist exhibited better thermodynamic stability and dispersion than the magnetite nanoparticles. Furthermore, the particle size and magnetic properties of the $[SiO_2\ (OH)_2]_8(N_2)_8$ composite nanoparticles can be controlled by changing the functional groups. The electrical properties such as NMR Shielding, electron densities, energy densities, potential energy densities, ELF, LOL, of electron density, eta index, ECP, ESR and hyperfine interactions for $Fe_3O_4$@ $[SiO_2(OH)_2]_8(N_2)_8$ have been calculated. As the catalyst could be easily recovered by magnetic separation and recycled for a few times without significant loss of its catalytic activity, we have calculated to obtain the stronger non bonded interaction in the $Fe_3O_4$@ $[SiO_2(OH)_2]_8(N_2)_8$ system. This system can be used for antibiotics drug delivery instead of injection. The chemical shielding and several factors as the same electronegativity, magnetic anisotropy of π-systems will be changed due to the number of electrons The chemical shielding is a vector orientation function for all of the shielding parameters that can change in several places inside the shielding region .

KEYWORD: super-paramagnetic Nano particle, QM/MM simulation, Fe3O4, $[SiO_2\ (OH)_2]8$, non-bonded interactions

*Department of Chemistry, Science and Research Branch, Islamic Azad University, Tehran, Iran

**Department of Chemical Engineering, Central Tehran Branch, Islamic Azad University, Tehran, Iran. E-mail: Maj.monajjemi@iauctb.ac.ir

Recibido: 29/04/2020 Aceptado: 17/06/2020

# Suministro de fármacos a través de paramagnéticos (N2) n [SiO2 (OH) 2] 8 Catalizador Core-Shell

RESUMEN

Los catalizadores MNPs @ [SiO2 (OH) 2] 8 se establecieron mediante simulación ab-initio y mecánica cuántica y mecánica molecular (QM / MM). Los estudios se centran en cómo mejorar la dispersión de partículas compuestas para lograr altos rendimientos magnéticos. Los resultados revelaron que el Fe3O4 @ [SiO2 (OH) 2] 8 (N2) 8 como cabalista exhibió una mejor estabilidad y dispersión termodinámica que las nanopartículas de magnetita. Además, el tamaño de partícula y las propiedades magnéticas de las nanopartículas compuestas [SiO2 (OH) 2] 8 (N2) 8 se pueden controlar cambiando los grupos funcionales. Las propiedades eléctricas tales como NMR Shielding, densidades de electrones, densidades de energía, densidades de energía potencial, ELF, LOL, de densidad de electrones, índice eta, ECP, ESR e interacciones hiperfinas para Fe3O4 @ [SiO2 (OH) 2] 8 (N2) 8 han sido calculados. Como el catalizador podría recuperarse fácilmente mediante separación magnética y reciclarse varias veces sin una pérdida significativa de su actividad catalítica, hemos calculado obtener la interacción no unida más fuerte en el sistema Fe3O4 @ [SiO2 (OH) 2] 8 (N2) 8. Este sistema se puede usar para la administración de antibióticos en lugar de la inyección. El blindaje químico y varios factores como la misma electronegatividad, la anisotropía magnética de los sistemas π se cambiarán debido a la cantidad de electrones. El blindaje químico es una función de orientación vectorial para todos los parámetros de blindaje que pueden cambiar en varios lugares dentro de la región de blindaje.

PALABRAS CLAVE: nanopartículas superparamágicas, simulación QM / MM, Fe3O4, [SiO2 (OH) 2] 8, interacciones no unidas

## Introduction

Since the magnetism in $Fe_3O_4$ was discovered, the material revolutionized the area of science with its wonderful properties. The materials have been at the core of the tremendous application such as electric motor, electromagnet, transformer, video/audiotape, and biomedical technologies etc. $Fe_3O_4$ is an electronic conductor with conductivities extremely higher than $Fe_2O_3$, and this is ascribed to electron exchange between the $Fe^{III}$ and $Fe^{II}$ centers. It is ferromagnetic with a curie temperature of 855 K and the ferromagnetism properties of $Fe_3O_4$ arises because the electron spin of both iron ions in the octahedral structures is coupled and the

spin of the $Fe^{3+}$ in the tetrahedral structure is coupled but anti-parallel to the previous one. This magnetic particle also falls under the categories of such functional materials owing to its several wonderful properties such as high Curie temperature (~850 K), and low electronic resistivity at lab temperatures. $Fe_3O_4$ is an important catalyst in the Haber process in the water gas shift reaction (Farhami, 2017). The latter uses a high temperature shift catalyst (HTS) of iron oxide stabilized by chromium oxide. This iron-chrome catalyst is reduced at reactor start up to generate $Fe_3O_4$ from $\alpha$-$Fe_2O_3$ & $Cr_2O_3$ to $CrO_3$. These kind magnetite particles are the earliest discovered magnet that crystallizes in the inverse cubic spinel structures. Each cubic spinel cell contains eight interpenetrating oxygen and the tetrahedral sites, occupied by one-third of the iron atoms, form a diamond structures. The remaining Fe atoms are located at the octahedral sites with the nearest-neighbor atoms lined up as strings along six different {110} directions. In other words $Fe_3O_4$ consists of a cubic close packed array of oxide ions where all of the $Fe^{2+}$ ions occupy half of the octahedral sites and the $Fe^{3+}$ are split evenly across the remaining octahedral sites and the tetrahedral sites. In this work we have investigated the catalysis's properties of Fe3O4 nanoparticles @[SiO2 (OH)2]8 to compare with $[SiO_2(OH)_2]_8(N_2)_8$ in the area of silicon effects of chemical synthesizes while the nano-$Fe_3O_4$@SiO2 supported ionic liquid Fe3O4@SiO2-IL can be successfully applied for perform the reaction of organic molecules (Bourgeois, 2000).

## 1. Computational details

Part of the systems including Fe3O4@ $[SiO2 (OH)_2]_8$, Fe3O4@ $[SiO_2(OH)_2]_8(N2)_8$ (Fig.1) and $Fe_3O_4$@SiO2-IL nanoparticles have been modeled with QM/MM method and the calculations are carried out with the DFT methods. In this investigation, differences in force field are illustrated by comparing the calculated energies with AMBER and OPLS force fields. Furthermore, Hyper-Chem professional release 7.01 programs applied for the additional calculations. For non-covalent interactions between core and shell, the B3LYP method is unable to describe van der Waals by medium-range interactions. Therefore, the ONIOM methods including 3 levels of 1-high calculation (H), 2-medium calculation (M), and 3-low calculation (L) have been performed in our study for calculating those non-bonded interactions (Frackowiak, 2002 ).

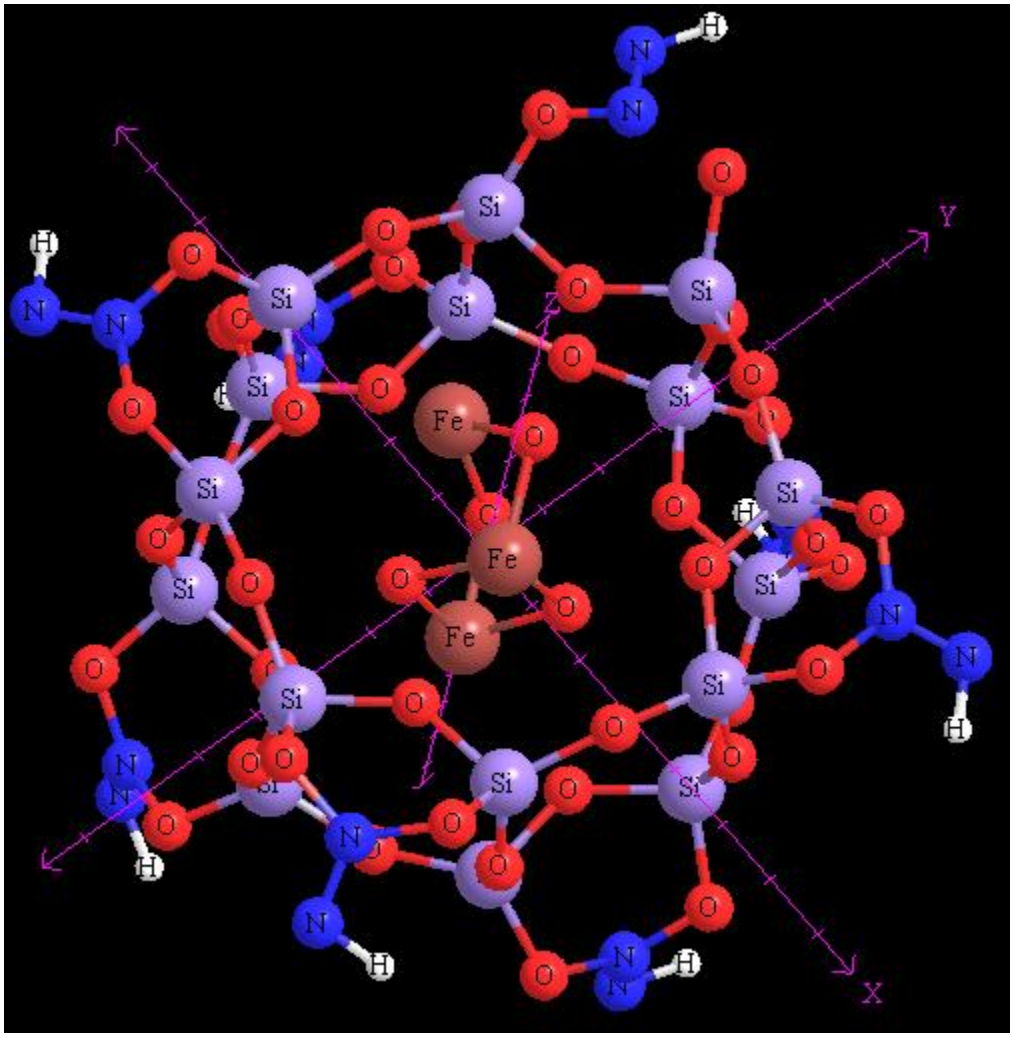


Fig.1.Non bonded interaction between Various Optimized $SiO2(OH)2]8(N2)n\ (n = 0 - 8)$ of core-shell nanoparticles.

The ab-initio and DFT methods are used for the model system of the ONIOM layers and the semi empirical methods of pm6 (including pseudo=lanl2) and Pm3MM are used for the medium and low layers, respectively **(**Monajjemi, 2009**)**. B3LYP and the most other popular and widely used functional are insufficient to illustrate the exchange and correlation energy for distant non-bonded medium-range systems correctly. Moreover, some recent studies have shown that inaccuracy for the medium-range exchange energies leads to large systematic errors in the prediction of molecular properties. Geometry optimizations and electronic structure calculations have been carried out using the m06 (DFT) functional. This approach is based on an iterative solution of the Kohn-Sham equation of the density functional theory in a plane-wave

set with the projector-augmented wave pseudo-potentials. The Perdew-Burke-Ernzerhof (PBE) exchange-correlation (XC) functional of the generalized gradient approximation (GGA) is also used. The optimizations of the lattice constants and the atomic coordinates are made by the minimization of the total energy (Monajjemi, 2011).

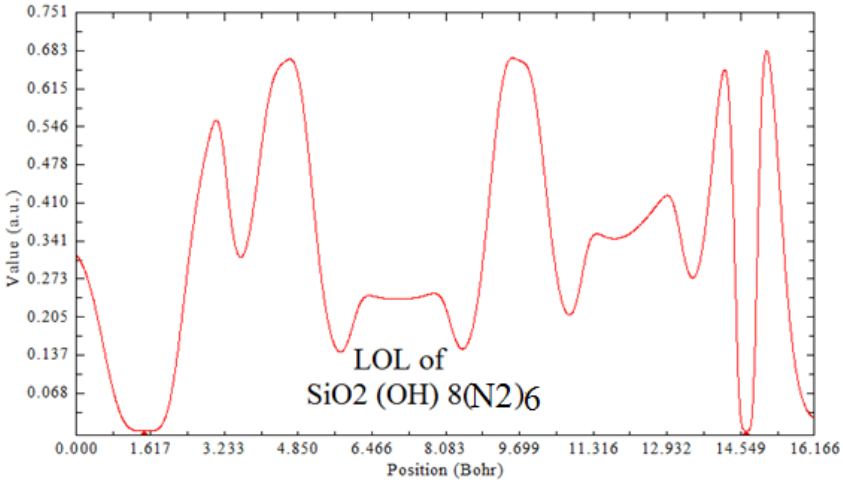


Fig.2: LOL for system of SiO2 (OH) 8(CO)x { X=6}

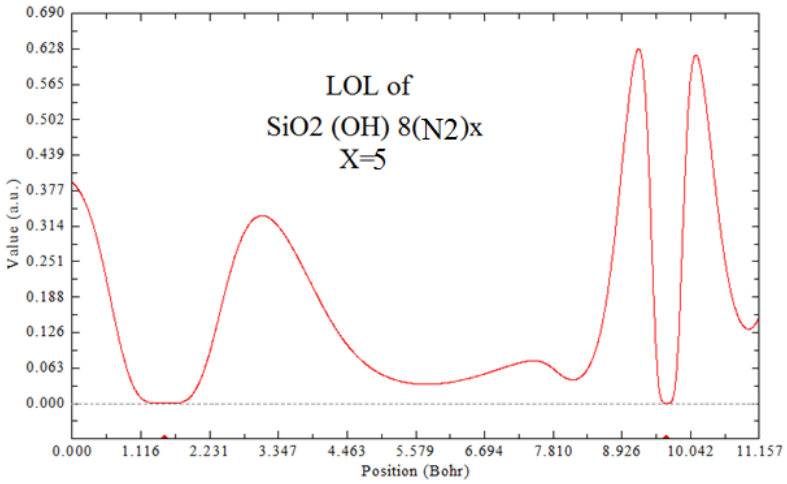


Fig.3: LOL for two systems of SiO2 (OH) 8(N2) x {X=5 }

The charge transfer and electrostatic potential-derived charge were also calculated using the Merz-Kollman-Singh Chelp or chelpG the charge calculation methods based on molecular electrostatic potential (MESP) fitting are not well-suited for treating larger systems whereas some of the innermost atoms are located far away from the points at which the MESP is computed. In such a condition, variations of the innermost atomic charges will not head towards

a significant change of the MESP outside of the molecule, meaning that the accurate values for the innermost atomic charges are not well-determined by MESP outside the molecule (Madani, 2017). The representative atomic charges for molecules should be computed as average values over several molecular conformations.

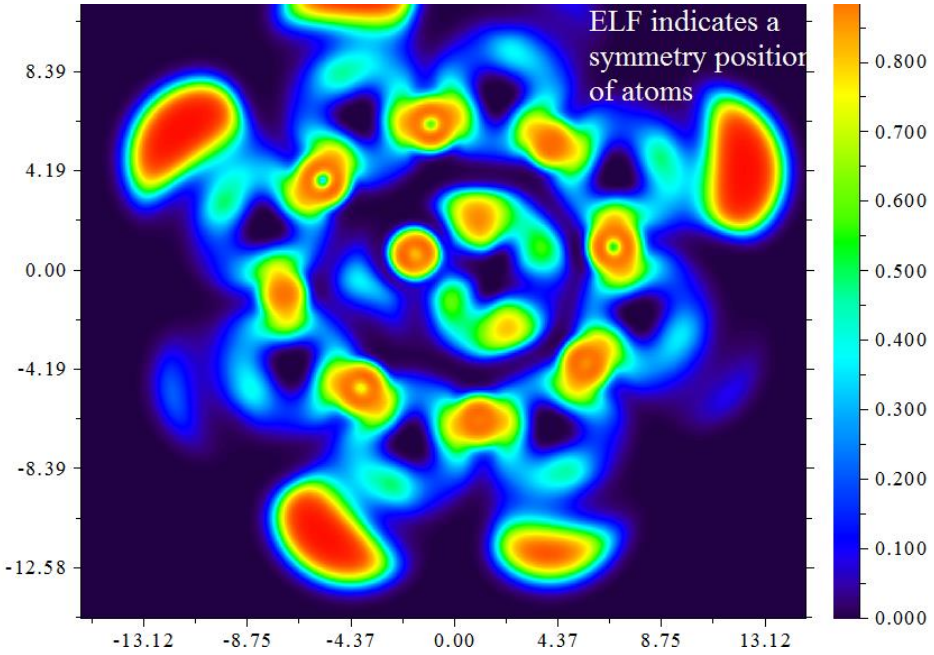


Fig.4. Color-field map of ELF for complexes [SiO2 (OH)2]8 (N2)4 indicates a symmetry position of systems

A detailed overview of the effects of the basis set and the Hamiltonian on the charge distribution can be found in references. The charge density profiles in this study has been extracted from first-principles calculation through an averaging process as described in reference. The interaction energy for capacitor was calculated in all items according to the equation as follows:

$$\Delta E_S(eV) = \{E_C - (\sum_{i=1}^{n}(Fe3O4 - [\mathrm{SiO2(OH)2]8(N2)n\ (n = 0 - 8)} + \sum_{i=6}^{14}(Fe3O4 - \mathrm{SiO2(OH)2]8(N2)n\ (n = 0 - 8)\}} \quad (1)$$

Where the "$\Delta E_S$" is the no bonded and stability energies of systems. The electron density (Both of Gradient norm & Laplacian), value of orbital wave-function, electron spin density, electrostatic potential from nuclear atomic charges, electron localization function (ELF), localized orbital locator (LOL defined by Becke & Tsirelson), total electrostatic potential

(ESP), as well as the exchange-correlation density, correlation hole and correlation factor, and the average local ionization energy using the Multifunctional Wave-function analyzer have also been calculated in this study. The contour line map was also drawn using the Multiwfn software (Lu, T., Chen, F., 2012). The solid lines indicate positive regions, while the dash lines indicate negative regions. The contour line corresponding to VdW surface (electron density=0.001 a.u., which is defined by R. F. W Bader) is plotted in this study. This is specifically useful to analyze distribution of electrostatic potential on VdW surface. Such a contour line has also been plotted in gradient line and vector field map by the same option. The relief map was used to present the height value at every point. Shaded surface map and shaded surface map with projection are used in our representation of height value at each situation (Frackowiak, 2002).

## 2. Theoretical background

### 2.1. The electron density

The electron density has been defined as $\rho(r) = \eta_i \left|\varphi_i(r)\right|^2 = \sum_i \eta_i \left|\sum_l C_{l,i}\,\chi_i(r)\right|^2$(2). [119-121] Where $\eta_i$ is occupation number of orbital (*i*), $\varphi$ is orbital wave function, $\chi$ is basis function and *C* is coefficient matrix, the element of $i_{\text{th}}$ row $j_{\text{th}}$ column corresponds to the expansion coefficient of orbital *j* respect to basis function *i*. Atomic unit for electron density can be explicitly written as e/Bohr$^3$. $\nabla\rho(r) = [(\frac{\partial\rho(r)}{\partial(x)})^2+(\frac{\partial\rho(r)}{\partial(y)})^2+(\frac{\partial\rho(r)}{\partial(z)})^2]^{\frac{1}{2}}$ (3) $\nabla^2\rho(r) = \frac{\partial^2\rho(r)}{\partial x^2} + \frac{\partial^2\rho(r)}{\partial y^2} + \frac{\partial^2\rho(r)}{\partial z^2}$(4)[18-20].

The positive and negative value of this function correspond to electron density is locally depleted and locally concentrated respectively. The relationships between $\nabla^2\rho$ and valence shell electron pair repulsion (VSEPR) model, chemical bond type, electron localization and chemical reactivity have been built by Bader.

### 2.2. Kinetic energy density K(r)

The kinetic energy density is not uniquely defined, since the expected value of kinetic energy operator $\langle \varphi \left| -\left(\frac{1}{2}\right)\nabla^2 \right| \varphi \rangle$ can be recovered by integrating kinetic energy density from

alternative definitions. One of commonly used definition is: $k(r) = -\frac{1}{2}\sum_i \eta_i \varphi_i^*(r)\nabla^2\varphi_i(r)$ **(5)**[119-121] Relative to *K*(r), the local kinetic energy definition given below guarantee positivizes everywhere; hence the physical meaning is clearer and is more commonly used. The Lagrangian kinetic energy density, "G(r)" is also known as positive definite kinetic energy density.

$G(r) = \frac{1}{2}\sum_i \eta_i \ |\nabla(\varphi_i|^{\ 2} = \frac{1}{2}\sum_i \eta_i\{[(\frac{\partial\varphi_i(r)}{\partial(x)})^2 + (\frac{\partial\varphi_i(r)}{\partial(y)})^2 + (\frac{\partial\varphi_i(r)}{\partial(z)})^2]\}$ **(6)**. *K*(r) and *G*(r) are directly related by Laplacian of electron density $\frac{1}{4}\nabla^2\rho(r) = G(r) - K(r)$ **(7)**.

## 2.3. Electron localization function (ELF)

Becke and Edgecombe noted that spherically averaged like spin conditional pair probability has direct correlation with the Fermi hole and then suggested electron localization function (ELF) [123]. ELF(r) $= \frac{1}{1+[D(r)/D_{0(r)}]^2}$ **(8)** where D(r) $= \frac{1}{2}\sum_i \eta_i \ |\nabla\varphi_i|^{\ 2} - \frac{1}{8}[\frac{|\ |\nabla\rho_\alpha|^{\ 2}}{\rho_\alpha(r)} + \frac{|\ |\nabla\rho_\beta|^{\ 2}}{\beta(r)}]$ **(9)** and $D_{0(r)} = \frac{3}{10}(6\pi^2)^{\frac{2}{3}}[\rho_\alpha(r)^{\frac{5}{3}} + \rho_\beta(r)^{\frac{5}{3}}]$ **(10)** for close-shell system, since $\rho_\alpha(r) = \rho_\beta(r) = \frac{1}{2}\rho$ , *D* and *D*0 terms can be simplified as D(r) $= \frac{1}{2}\sum_i \eta_i \ |\nabla\varphi_i|^{\ 2} - \frac{1}{8}[\frac{|\nabla\rho|^{\ 2}}{\rho(r)}]$ **(11)**, $D_{0(r)} = \frac{3}{10}(3\pi^2)^{\frac{2}{3}}\rho(r)^{\frac{5}{3}}$ **(12)**.

Savin *et al*. have reinterpreted ELF in the view of kinetic energy, which makes ELF also meaningful for Kohn-Sham DFT wave-function or even post-HF wave-function. They indicated that *D*(r) reveals the excess kinetic energy density caused by Pauli repulsion, while *D*0(r) can be considered as Thomas-Fermi kinetic energy density. Localized orbital locator (LOL) is another function for locating high localization regions likewise ELF, defined by Schmider and Becke in the paper[25]. $LOL(r) = \frac{\tau(r)}{1+\tau(r)}$ **(13)**, where $(r) = \frac{D_0(r)}{\frac{1}{2}\sum_i \eta_i \ |\nabla\varphi_i|^{\ 2}}$ **(14)**, $D_0(r)$ for spin-polarized system and close-shell system are defined in the same way as in ELF. Local information entropy is a quantification of information, this theory was proposed by Shannon in his study of information transmission in noise channel, and nowadays its application has been largely widened to other areas, including theoretical chemistry. Parr *et al.* discussed the relationship

between information entropy and atom partition as well as molecular similarity. This simulation and modeling of systems have been done based on our previous work.

## 3. Result and discussion

Modified magnetic materials are nowadays well-known and have been investigated intensively due to their potential applications in many areas, such as biology, medicine and the environment. These applications include enzyme and protein separations, RNA and DNA purifications (Deng, 2010).

The term "Ab Initio" is given to computations which are derived directly from theoretical principles, with no inclusion of experimental information. The most common type of ab initio calculation is called a Hartree-Fock calculation, in which the primary approximation is called the central field approximation. A method, which avoids making the HF mistakes in the first place, is known as Quantum Monte Carlo (QMC). Also, in contrast to the MD method which is entirely deterministic, the MC simulation method is based on the use of probabilistic concepts. In this method, a system composed of *N* interacting atoms is given a group of initial coordinates.

The evolution of this initial configuration is then generated by these successive random displacements of the atoms. There are some flavors of QMC vibrational, diffusion, and Green's functions. These methods work with a clearly correlated wave function and evaluate integrals numerically using a Monte Carlo integration. These calculations can be very time consuming, but they are apparently the most accurate methods known today. Ab initio calculations give very good qualitative results and can give increasingly accurate quantitative results as the molecules in question become smaller, generally. There are three steps in carrying out any quantum mechanical calculation in Hyper-Chem 8.0 program package. First, set up a molecule with an appropriate starting geometry. Second, choose a calculation method and its associated choices. Third, choose the type of calculation with the relevant options. The Monte Carlo simulations always detect the so-called "important phase space" regions which are of low energy. Because of defects of the force field, this lowest energy basin usually does not correspond to the native state in most cases, so the rank of native structure in those decoys produced by the force field itself is poor. In this study, difference in force field is illustrated by comparing the energy

calculated by using force fields, MM+, Amber, and OPLS. Also, we investigated polar solvent and the temperature effects (between 260K and 400K) on the stability of SWBNNT bonded to CFA (or CGA) in various solvents. The quantum mechanics (QM) calculations were carried out with the Hyper-Chem 8.0 program. This study mainly focuses on the magnetic properties of Fe3O4 in a non-bonded system with $SiO2(OH)2]8(N2)n\ (n = 0 - 8)$shell surfaces. The non-bonded interaction is shown in figs1- 8. As it is indicated in tables 1-10, the electrical properties can be obtained from changes in the non-bonded interactions. Electron densities, energy densities, Potential energy densities, ELF, LOL, Ellipticity of electron density, eta index and ECP for $SiO2(OH)2]8(N2)n\ (n = 0 - 8)$ were calculated of each simulation (Tables 1-10).

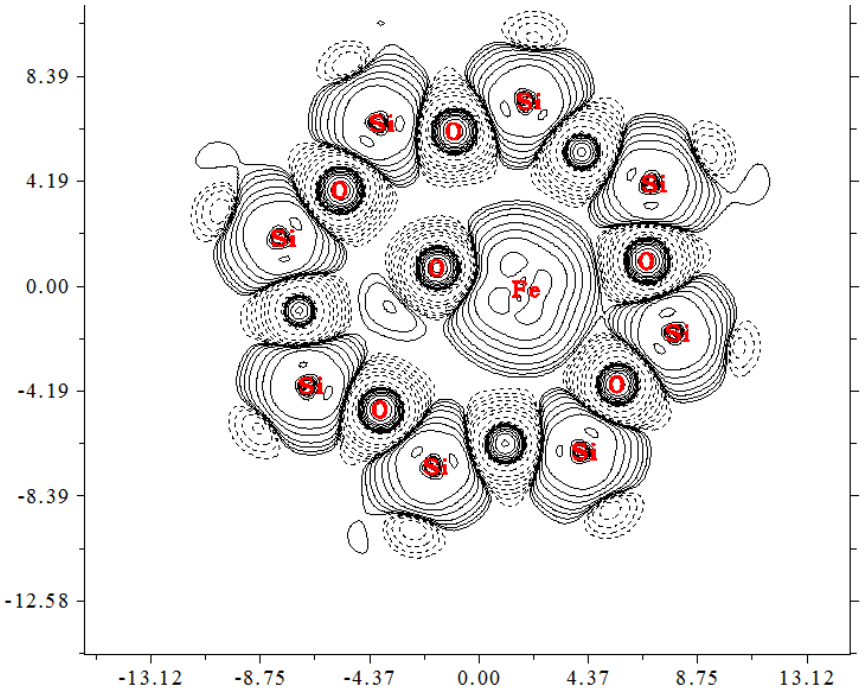


**Fig.5:** Density of Hamiltonian kinetic energy for [SiO2 (OH)2]8

According to the equation 13, 14 the largest electron localization is located on Fe3O4 where the electron motion is more likely to be confined within that region. If electrons are completely localized in the Fe3O4, they can be distinguished from the ones outside. As shown in tables 1-10 the large ELF is close to the Fe3O4 atoms. The regions with large electron localization need to have large magnitudes of Fermi-hole integration which would lead the Fe3O4 towards superparamagnetic. The fermi hole is a six-dimension function and as a result,

it is difficult to be studied visually. Based on equations 12, 13 and 14, Becke and Edgecombe noted that the Fermi hole is a spherical average of the spin which is in good agreement with our results in tables and Figs.

Table1: All Electron Densities of non-bonded interactions for $SiO2[(OH)2]8$complexes

| Atom(number) | Density of all electron($10^{-3}$) | Density of alpha ($10^{-3}$) | Density of Beta ($10^{-3}$) | Spin Density |
|---|---|---|---|---|
| Fe(1) | 0.29 | 0.16 | 0.16 | 0.0 |
| Fe(2) | 0.21 | 0.12 | 0.12 | 0.0 |
| Fe(3) | 0.33 | 0.15 | 0.14 | 0.01 |
| O(1) | 0.13 | 0.05 | 0.04 | -0.01 |
| O(2) | 0.25 | 0.15 | 0.15 | 0.0 |
| O(3) | 0.33 | 0.17 | 0.15 | 0.02 |
| O(4) | 0.21 | 0.14 | 0.13 | -0.02 |

Table.2: Gap energies for various [SiO2 (OH) ]8(N2)n (n=0-8)

| [SiO2(OH)2]8 (N2)n | HOMO (e.V) | LUMO (e.V) | Gapenergy (e.V) |
|---|---|---|---|
| n=0 | -3.234562 | -0.234515 | 3.000047 |
| n=1 | -3.956745 | -0.298765 | 3.65798 |
| n=2 | -3.879656 | -0.287659 | 3.591997 |
| n=3 | -3.873456 | -0.234987 | 3.636489 |
| n=4 | -3.768545 | -0.277531 | 3.491014 |
| n=5 | -3.150873 | -0.254573 | 2.896300 |
| n=6 | -3.457843 | -0.298342 | 3.159501 |
| n=7 | -3.376543 | -0.232485 | 3.144058 |
| n=8 | -3.768456 | -0.309566 | 3.458890 |

ELF indicates that it is actually a relative localization and must be accounted within the range of [0, 1]. A large ELF value corresponds to largely localized electrons which indicate that a covalent bond, a lone pair or inner shells of the atom is involved. According to equation 16, LOL can be interpreted similar to ELF in terms of kinetic energy, though; LOL can also be interpreted in terms of localized orbitals. Small (large) LOL value usually appears in boundary (inner) region of localized orbitals due to the large (small) gradient of orbital wave-function in this area. The value range of LOL is identical to ELF, namely [0, 1]. LOL has a similar expression as ELF.

Table3: Energies of non-bonded interactions for Fe3O4@ [SiO2 (OH)2]8 (N2)4

| [SiO2(OH)2]8 (N2)4 | Lagrangian kinetic [G(r)]energy($10^{-3}$) | Hamiltonian kinetic [K(r)]energy($10^{-2}$) |
|---|---|---|
| Fe(1) | 0.35 | 0.46 |
| Fe(2) | 0.36 | 0.37 |
| Fe(3) | 0.34 | 0.41 |
| O(1) | 0.13 | -0.13 |
| O(2) | 0.16 | -0.17 |
| O(3) | 0.22 | -0.24 |
| O(4) | 0.24 | -0.25 |

Table4: Laplacian, ELF, LOL and Local information entropy of non-bonded interactions of Fe3O4@ [SiO2 (OH)2]8 (N2)4

| Atom(number) | Laplacian of electron density($10^{-1}$) | Electron localization function (ELF) ($10^{-3}$) | Localized orbital locator (LOL) ($10^{-1}$) | Local information entropy ($10^{-4}$) |
|---|---|---|---|---|
| Fe(1) | -0.21 | 0.44 | 0.13 | 0.56 |
| Fe(2) | -0.31 | 0.41 | 0.34 | 0.19 |
| Fe(3) | -0.35 | 0.16 | 0.23 | 0.25 |
| O(1) | 0.13 | 0.51 | 0.23 | 0.22 |
| O(2) | 0.41 | 0.16 | 0.55 | 0.35 |
| O(3) | 0.36 | 0.42 | 0.21 | 0.40 |
| O(4) | 0.15 | 0.21 | 0.43 | 0.20 |

As it is indicated in tables, LOL is low and constant for those $SiO2(OH)2]8(N2)n(n = 0 - 8)$ compounds. The results of ELF and LOL indicate that the Fe3O4 starts to act as a super magnetic in any situation inside of shell.

Table5: Average local ionization energy, RDG and ESP of non-bonded interactions for Fe3O4@ [SiO2 (OH)2]8 (N2)3

| Atom(number) | Reduced density gradient(RDG) $(10^{+1})$ | Average local ionization energy | ESP from nuclear charge $(10^{4})$ | ESP from electron charge $(10^{2})$ |
|---|---|---|---|---|
| Fe(1) | 0.42 | 0.43 | 0.13 | -0.17 |
| Fe(2) | 0.35 | 0.56 | 0.15 | -0.50 |
| Fe(3) | 0.41 | 0.31 | 0.11 | -0.45 |
| O(1) | 0.23 | 0.60 | 0.17 | -0.14 |
| O(2) | 0.24 | 0.21 | 0.16 | -0.43 |
| O(3) | 0.35 | 0.35 | 0.13 | -0.33 |
| O(4) | 0.23 | 0.16 | 0.12 | -0.31 |

Table6: Lambada2, Wave function value, Ellipticity of electron density and Eta index of non-bonded interactions for Average local ionization energy, RDG and ESP of non-bonded interactions for Fe3O4@ [SiO2 (OH)2]8 (N2)2

| Atom(number) | Lambada2 $(10^{-3})$ | Wave function value $10^{-4})$ | Ellipticity of electron density | Eta index |
|---|---|---|---|---|
| Fe(1) | -0.25 | 0.84 | 0.42 | -4.3 |
| Fe(2) | -0.24 | 0.73 | 0.45 | -1.3 |
| Fe(3) | -0.22 | 0.60 | 0.43 | 0.80 |
| O(1) | 0.18 | 0.51 | -0.14 | 0.75 |
| O(2) | 0.25 | 0.53 | -0.26 | 0.52 |
| O(3) | 0.23 | 0.42 | -0.17 | 0.43 |
| O(4) | 0.23 | -0.37 | -0.24 | 0.31 |

As it is shown in Fig1-10, there are fluctuations within a decreasing amount for electron density, energy density, ELF and LOL, while there is no fluctuation for ESP which is actually periodic.

Currently, a number of drugs are used in the treatment of the cancer, but most of them were produced controlled effect on the cancer cells. The usual applications of hetero-cycles are as vast as it is diverse and is not extensively encompassed in the scope of that study. The most drugs belong to a class of hetero-genius structures. Heterocyclic structures played an important behavior in the metabolism of all cells; maximum number of them is 6 (or sometimes 5) membered hetero-cycles including one to three hetero-atoms. Recently, imidazole fragment has been attracting much concentration because of its role as attractive scaffold for biochemical

active hetero-cyclic drugs. Generally, chemical-physics and biochemical properties like acceptor and donor capabilities, hydrogen bond, π-π interactions, van der Waals, coordination bond with a metal and in total hydrophobic force has caused much interest in anticancer studies for such compounds. These properties are important of understanding for its reactivity enable derivative for binding with various nucleic acids, enzymes and biological structures. A large number of the important heterocyclic compounds are used in the medical activities such as histidine and proline which are amino acids. It is notable pyridoxine, folic acid, thiamine, riboflavin, biotin, $B_{12}$ and E families of the vitamins are included of heterocyclic structures. For investigation of antifungal activity compounds, Singh et al have synthesized 1,3, 4oxadiazolo-(3,2a)-s-triazin-7-thione and Abdle,et-al have synthesized some novel 1, 3, 4oxadiazole derivatives. Fungi are hetero-tropic micro-organisms that are distinguished. Dhar has synthesized 1,3,4-oxadiazolo-[3,2-a]-1,3,4-dithiazines and found anti-fungal. In compound Ar=2- ClC6H4, Ar'=2-ClC6H4OCH2.Methyl 5- (l-hydroxy-2-propenyl)-3-thiophenecarboxylate was stirred at room temperature with 10 equivalents of freshly prepared manganese dioxide to give methyl 5-(2-propenoyl)-3- thiophene carboxylatein 60% yield. The proton nmr spectrum exhibit explicitly a doublets for two hydrogens due to the de-shielding effect of the carbonyl. Infra-red spectroscopy helps to confirm the structure of two carbonyls around 1650 $cm^{-1}$ for the allylic ketone and 1700 $cm^{-1}$ for the ester Figs1-3. Since a carcinogen is applied into a body, cancerous cell will not immediately result. This is due to the "latency effect" where certain of time elapses before there is growth of the tumor. The initial application of a carcinogen will result in the formation of the irreversible initiated cells. Time may then elapse before a second agent, known as the promoter, will act reversibly on the initiated cell giving a premalignant lesion. Changes in the premalignant lesion, such as increased growth rate, increased invasiveness and metastases, result from the 3$^{rd}$ stage of the process known as progression. Those changes are usually associated with the changing in the number and arrangement of genes which encode for various proteins.

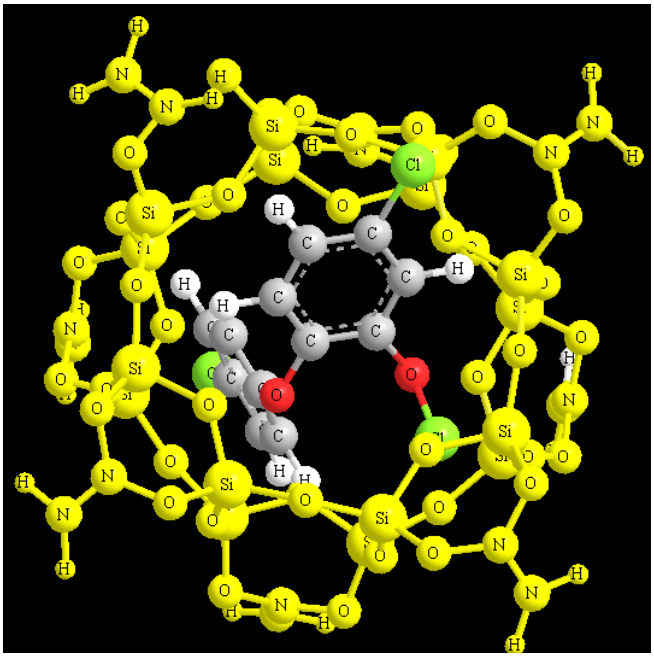

**Fig.6:** Tricloson antibiotic delivery via [SiO2 (OH)2]8

The chemical shielding and several factors as the same electronegativity, magnetic anisotropy of π-systems will be changed due to the number of electrons The chemical shielding is a vector orientation function for all of the shielding parameters that can change in several places inside the shielding region (Figs 6-11).

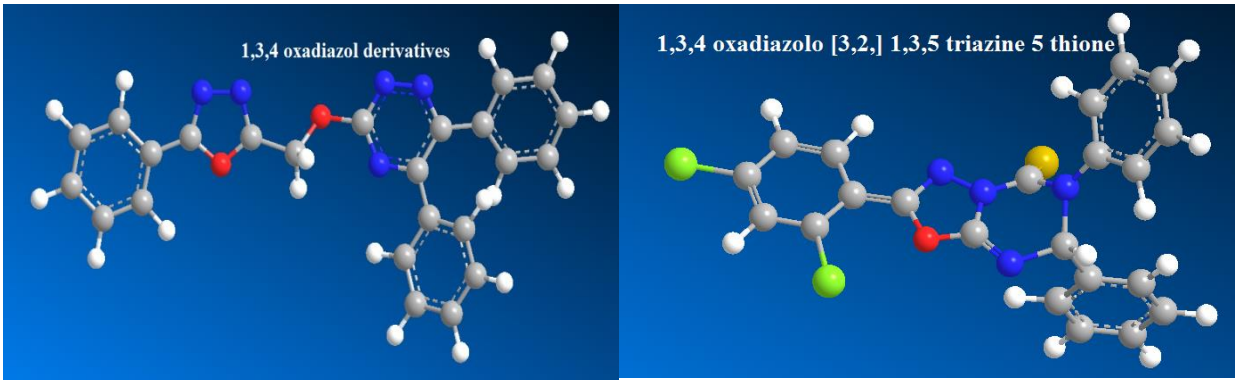


Fig.7. optimization of 1,3,4 oxadiazol derivatives and 1,3,4 oxadiazolo [3,2,] 1,3,5 triazine 5 thione

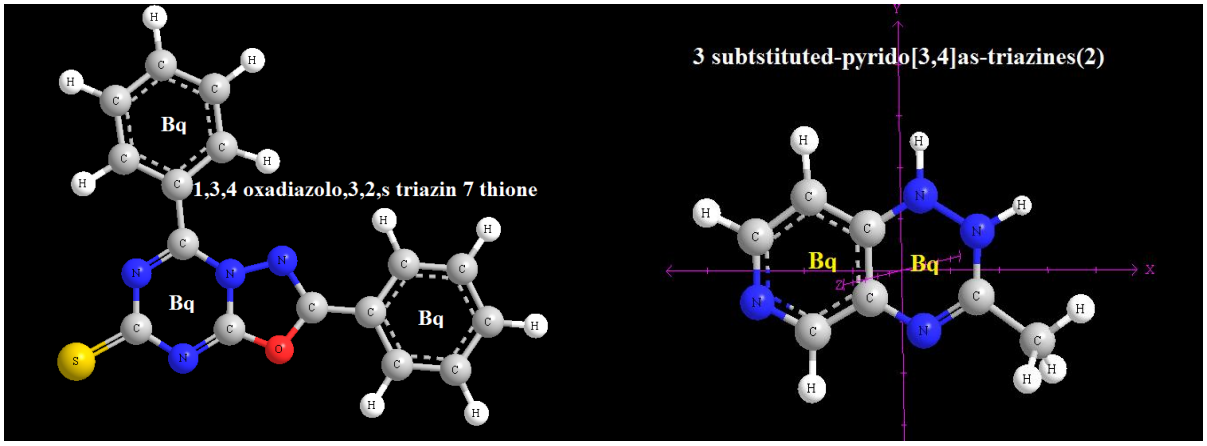


Fig.8. optimization of 1,3,4 oxadiazolo,3,2,s triazin 7 thione and 3 subtstituted-pyrido[3,4]as-triazines(2).

Optimization& NMR constants with orientations of the principal components& Haeberlen-Mehring, or Herzfeld-Berger parameter for several heterocyclic compounds in random situations has been calculated through DFT methods tables1, 2. In small distance around the center, the asymmetric-parameter (η), and the skew (**κ**), exhibited. gaussian distribution based on their fluctuation behavior[15], which is relate on its distance of molecular ring. In contrast, of that parameters, the isotropy $\sigma_{iso}(r)$ Has not a fluctuating behavior and increase in around the center of the rings with a linear relationship. The slopes of that line is changed for various distances of heterocyclic compounds. The isotropy in all NMR calculations are positive which indicates negative values for aromaticity.

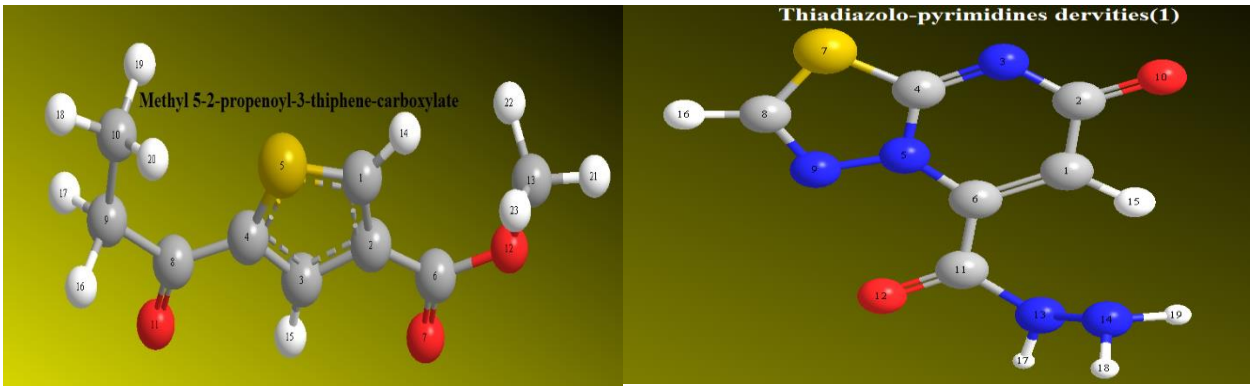


Fig.9. optimization of Methyl 5-2-propenoyl-3-thiphene-carboxylate and Thiadiazolo-pyrimidines derivatives (1)

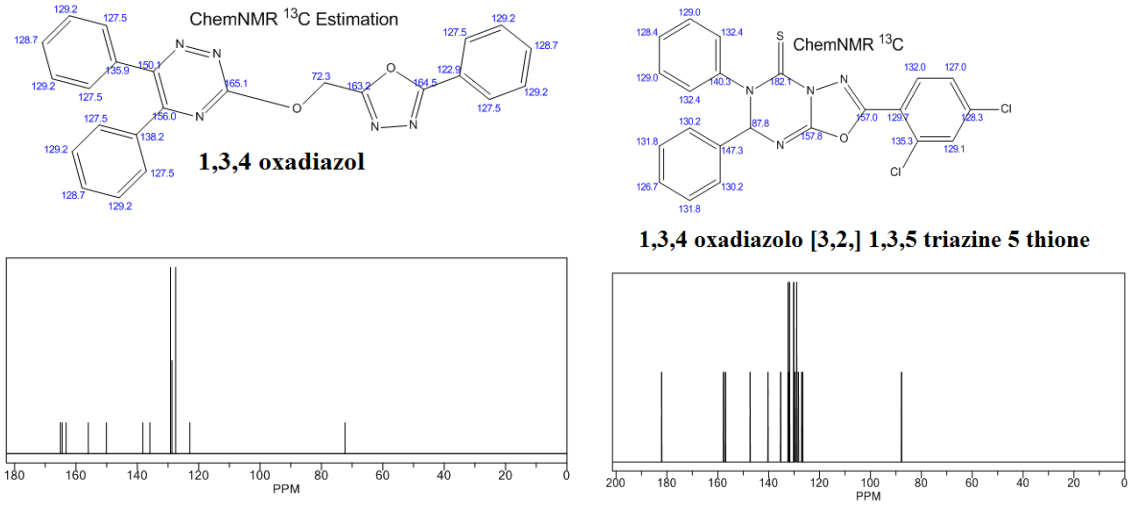


Fig.10. NMR estimation of some oxadiazol compounds

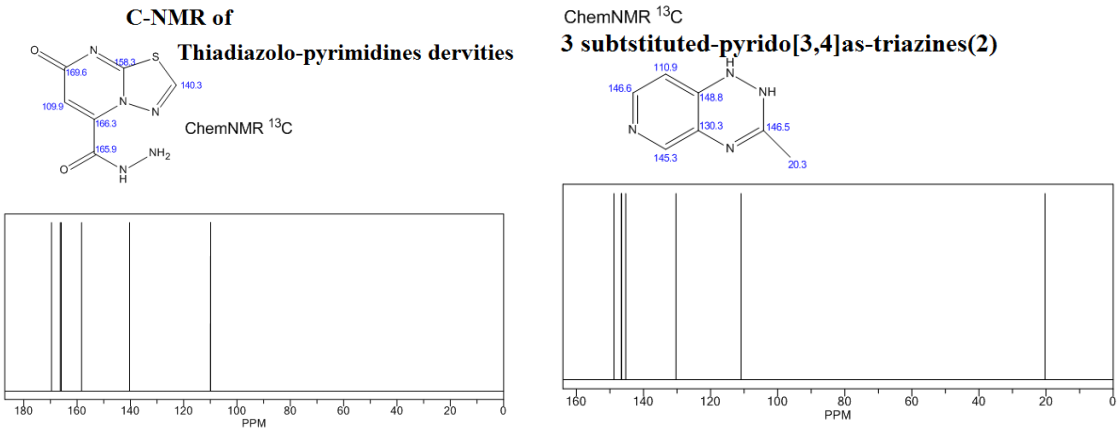


Fig.11. NMR estimation of some Thiadiazol compounds

## Conclusion

Once a compound that fulfills all of these requirements has been identified, it will begin the process of drug development prior to clinical trials. Modern drug discovery involves the identification of screening hits, medicinal chemistry and optimization of those hits to increase some properties. One or more of these steps may involve computer-aided drug design and drug-delivery via silica compounds such as $(N2)n[SiO2(OH)2]8$ Core-Shell catalyst. A fascinating result of the theoretical analysis of antibiotics- S-NICS methods were the stable model for drug delivery. The observed behavior must reflect intrinsic properties of the mechanism of its structure and provides useful constraints for the development of mechanistic models.

## References

Bourgeois, L., Bando, Y., Han, W.Q., Sato, T. (2000). Structure of boron nitride nanoscale cones: Ordered stacking of 240° and 300° disclinations *Phys. Rev*. B, (61), 7686.

Deng, Y.; Cai, Y.; Sun, Z.; Liu, J.; Liu, C.; Wei, J.; Li, W.; Liu, C.; Wang, Y.; Zhao, D.; (2010). Multifunctional Mesoporous Composite Microspheres with Well-Designed Nanostructure : A Highly Integrated Catalyst System, J. AM. CHEM. SOC., *132*, 8466–8473.

Farhami, N., Monajjemi, M., Zare, K. (2017). Non Bonded Interactions in cylindrical capacitor of (m, n) @ (m', n') @ (m",n") Three Walled Nano Carbon Nanotubes. *Oriental Journal of Chemistry* (*33*), 3024- 3030, http://dx.doi.org/10.13005 /ojc/ 330640

Frackowiak, E., Béguin, F. (2002). Electrochemical storage of energy in carbon nanotubes. *Carbon*, *(40)*, 1775-1787, https://doi.org/10.1016/S0008-223(02)00045-3

Iijima Sumio (1991). Synthesis of Carbon Nanotubes. *Nature*, (354), 56-58.

Lee, V.S., Nimmanpipug, P.,Mollaamin, F., Kungwan, N., Thanasanvorakun, S., Monajjemi, M.(2009). Investigation of single wall carbon nanotubes electrical properties and mode analysis: Dielectric effects. *Russian journal of physical chemistry A* (*83*), 2288-2296, https://doi.org/10.1134/S0036024409130184.

Lu, T., Chen, F. (2012). Multiwfn: A Multifunctional Wavefunction Analyzer. *J. Comp. Chem*., *33*, 580-592, https://doi.org/10.1002/jcc.22885.

Madani, M.S., Monajjemi, M., Aghaei, H. (2017), The Double Wall Boron Nitride Nanotube: Nano-Cylindrical Capacitor, *Oriental Journal of Chemistry*, (*33*), 1213-1222 , http://dx.doi.org/10.13005/ojc/330320.

Monajjemi, M., Chegini, H., Mollaamin, F., Farahani, P. (2011). Theoretical Studies of Solvent Effect on Normal Mode Analysis and Thermodynamic Properties of Zigzag (5,0) carbon nanotube. *Fullerens Nanotubes carbon and nanostructures* (*19*), 469-482, https://doi.org/10.1080/1536383X.2010.494783.